IEEE Open Access Journal of
Power and Energy

Received 15 July 2022; revised 4 September 2022 and 27 December 2022; accepted 29 December 2022.
Date of publication 5 January 2023; date of current version 14 February 2023.

Digital Object Identifier 10.1109/OAJPE.2023.3234468

An Online Multi-Level Energy Management System for Commercial Building Microgrids With Multiple Generation and Storage Systems

WENSHUAI BAI[1], DIAN WANG[2], XIAORONG SUN[1], JIABIN YU[1], JIPING XU[1], AND YUQING PAN[1]

[1]School of Artificial Intelligence, Beijing Technology and Business University, Beijing 100048, China
[2]Energy Internet Research Department, State Grid Energy Research Institute Company Ltd., Beijing 102209, China

CORRESPONDING AUTHOR: W. BAI (baiwenshuai@btbu.edu.cn)

This work was supported by the Research Foundation for Youth Scholars of Beijing Technology and Business University under Grant QNJJ2022-40.

ABSTRACT This paper presents an online multi-level energy management system for local microgrids of commercial buildings that integrate roof-top photovoltaic sources, battery storage systems, utility grids, diesel generators, supercapacitors, and commercial buildings consisting of active orchestrated loads, to solve the uncertainty problem of sources and loads, while also optimizing the local microgrid operation cost of commercial buildings and the utilization rate of local renewable energy. The energy management system includes a long-term rolling optimization level, rule-based optimization level, and load demand optimization level. At the long-term rolling optimization level, an online rolling method of data restructuring is proposed, where measurement data, short-term prediction data, and day-ahead prediction data are reconstructed to reduce the uncertainty in photovoltaic source prediction and load demand prediction. Four methods are proposed for the energy management system and simulated in MATLAB/Simulink under three typical weather conditions, cloudy, sunny, and rainy. Simulation results show that the performance of Method 3 is closest to that of Method 4, whose data conditions are ideal; Method 3 reduces the operational cost of the commercial building microgrid and improves the utilization rate of photovoltaic sources, at the slight cost of non-critical load shedding.

INDEX TERMS Commercial buildings, online, energy management system, microgrids, operational cost, utilization rate.

I. INTRODUCTION

THE building sector accounts for almost 55% of global electricity consumption and approximately 37% of global CO_2 emissions [1]. In buildings, the potential for enormous emission reductions remains untapped owing to the continued use of fossil-fuel-based assets, a lack of effective energy-efficiency policies, and insufficient investment [2]. Commercial buildings, such as offices and banks, widely exist in urban areas and account for much of the overall load demand. Such buildings are characterized by the load demand changing with the workday, with the load demand peaking during the daytime. Coincidentally, photovoltaic (PV) sources generate power in the daytime and can supply power to the aforementioned buildings, which is a potential way to achieve net-zero energy consumption. In line with the concept of green buildings, the daily power consumption of buildings can be guaranteed by configuring reasonable PV sources and battery storage (BS) [3].

With the development of green buildings equipped with a roofed PV system, there is increased interest in studying an energy management system (EMS) in terms of the uncertainty in renewable power generation [4], [5], [6] and the load demand [7], [8], [9]. Methods of addressing uncertainties considering both the demands and supplies of microgrids can be categorized into two types. The first type is non-deterministic modeling methods that model uncertainties

through probabilistic statistical methods. In [10], PV solar power uncertainty was analyzed with solar power scenario generation and reduction methods based on the Wasserstein distance metric and K-medoids, respectively, and the generation of solar power was obtained using a probability distribution function. In [11], the Gaussian probability distribution function was used to simulate uncertainty scenarios for demands. In [12], the beta and Rayleigh probability density functions were used to model uncertainties in solar irradiance and wind speed, respectively. In [13], lognormal distributions were applied to model EV uncertainties. The advantage of the non-deterministic modeling method is that uncertainties can be modeled based solely on statistical data avoiding building complex physical models. The drawback of the method is that it is difficult to obtain an appropriate probability density function and the prediction error of short-term data maybe increase due to its non-stationary characteristic, therefore, it is more suitable for intra-day predicted data. The second type is deterministic modeling methods that usually use a non-probabilistic model to reduce the uncertainty by improving the data prediction accuracy; such as the time-series prediction method and neural network method. In [14], a neural network was applied to predict the load demand with a feed-forward structure. In [11], the autoregressive moving-average model was used to predict wind generation. In [15], the traditional encoder single deep learning method was introduced for weather forecasts using deep learning techniques. In [16], boosted decision tree regression model was applied to predict the changes in solar radiation based on collected data in Malaysia. In [17], an optimal scheduling model was proposed for isolated microgrids by using automated reinforcement learning-based multi-period forecasting of renewable power generations and loads to reduce the negative impact of the uncertainty of load and renewable energies outputs on microgrid operation. In [18], an elman neural network prediction model is developed for load forecasting. The advantage of the deterministic modeling method is that the model can run fast to get online accessible results. The disadvantage of this method is that it is difficult to obtain accurate long-term data, therefore, it is more suitable for intra-hour predicted data. Considering the online operation requirements of a commercial building microgrid in this paper, the deterministic modeling method is applied to deal with the uncertainty of local renewable energy and loads. Weather data obtained from official weather forecast agency and the deterministic modeling method are then combined to predict long-term online data, which not only saves forecast time but also inherits the prediction accuracy.

To further resolve the uncertainty, an EMS integrated into a microgrid was proposed to improve the flexibility, stability, and reliability of a power supply [19], [20]. The EMS plays a critical role in determining the economy and environmental friendliness of commercial building microgrids. Reference [21] proposed an optimal EMS for a direct current (DC) microgrid applied to a commercial building, with the EMS

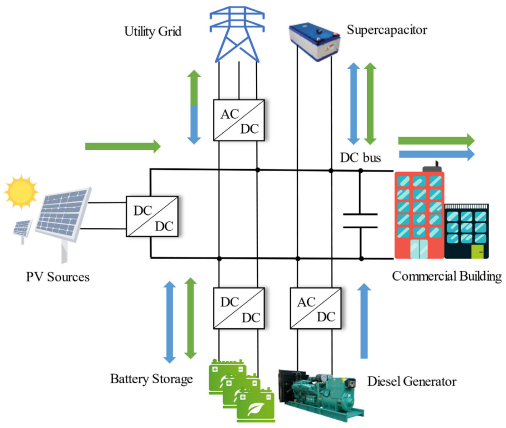

FIGURE 1. Microgrid topology of a commercial building.

contributing to power quality, fuel savings, and power efficiency, but the study does not consider economic aspects of the EMS, such as electricity prices, which directly affect the demand response of commercial buildings. In [22], a model predictive control algorithm for the EMS in an apartment building integrating a microgrid was proposed to reduce the electricity bill of a building and to improve the matching of local generation and consumption. However, the simplistic optimization objective only considers the power cost of the utility grid (UG) and does not improve the usage rate of renewable energy sources (RESs) or the power cost of the storage system. Reference [23] presented a model for the EMS of a building microgrid coupled with a battery that was modeled considering battery degradation and real-life operation characteristics. The proposed model could reduce the building owner's annual cost by up to 3.1% under the considered pricing scheme but does not consider the usage rate of RESs. In [24], a novel structure for parking lot microgrids was proposed to guarantee demand flexibility, minimize the electricity consumption cost for the owners of electric vehicles (EVs), and make a profit for the microgrid; however, the proposed structure is limited to using only day-ahead peak-shaving and valley-filling for power systems with distinct peak hours in the daily operation and does not consider the intraday uncertainty of the renewable power generation and load demand, which affects the performance of the intraday system, including the economy and RES utilization.

Against the above background, this paper proposes an online multi-level EMS for commercial building microgrids with multiple sources and a series of interruptible appliances to consider long-term energy planning while maintaining the real-time supply-demand balance.

A microgrid shall have the capability to be isolated. While conventional microgrids emphasize their role as a way to improve local energy independence and resilience, commercial building microgrids typically maintain power supply for at least enough time to cope with UG outages without damaging the system, and even in some cases, they may be able to

power the system indefinitely [25], [26]. The microgrid topology of a commercial building, shown in Fig. 1, comprises PV sources, a UG, BS, a diesel generator (DG), a supercapacitor (SC), and a commercial building. The proposed EMS adopts rolling optimization to deal with the uncertainty in PV power generation and the load demand online. The error in the rolling optimization can be rescheduled online at the rule-based level of the EMS. The main contributions of this paper are as follows:

1) An online multi-level EMS, including a long-term rolling optimization level, rule-based optimization level, and load demand optimization level, is designed in this paper to consider long-term energy planning while maintaining the real-time supply-demand balance. In the load demand optimization level, a time-constrained and power-constrained load management method is applied according to the load priority.
2) At the long-term rolling optimization level, an online rolling method of data restructuring combining multiple types of data is proposed to improve the uncertainty in PV power generation and load demand.
3) Four methods are comprehensively analyzed and compared under three weather conditions for the EMS. Method 4, which does not consider uncertainty in PV power generation and the load demand power prediction, provides a powerful reference. Simulations show that Method 3 is effective in reducing the operational cost of the commercial building microgrid and improving the utilization rate of PV sources.

The remainder of the paper is organized as follows. Section II describes the studied online rolling method of reconstructing data. Section III presents the design processes of the multi-level EMS that comprises a long-term rolling optimization level, load demand optimization level, and rule-based optimization level. The multi-level EMS is validated in Section IV. Finally, conclusions and directions of future work are discussed in Section V.

II. ONLINE ROLLING METHOD OF DATA RESTRUCTURING

After comprehensively considering the modeling cost and modeling accuracy of the uncertainties, an online rolling method of data restructuring is proposed to construct prediction data for the load power and RES power by restructuring three types of data: day-ahead prediction data, short-term prediction data, and measurement data. As shown in Fig. 2, the structure of the online rolling method consists of five parts, where the four parts: a PV short-term prediction model, a load short-term prediction model, a PV day-ahead prediction model, and a load day-ahead prediction mode, provide the measurement data, the short-term prediction data and the day-ahead predicted data for the restructured data frame. The mathematical expression of this method is shown in (1), where the restructured data frame, F_{RS}, is denoted by the measurement data, M_{ti} (t_i is from t_m to t_0), the short-term prediction data, S_{ti} (t_i is from t_1 to t_s), and the day-ahead predicted data, D_{ti} (t_i is from t_{s+1} to t_d). δ is dirac delta function.

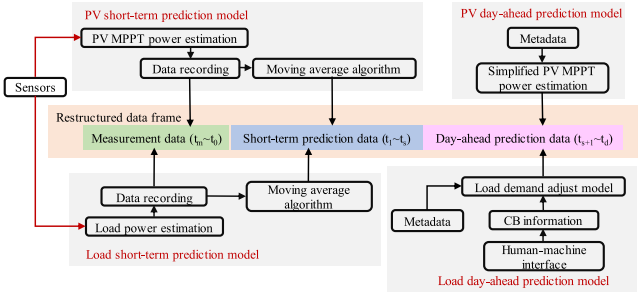

FIGURE 2. **Structure of the online rolling method.**

$$F_{RS} = \begin{cases} \sum_{i=m}^{0} M_{t_i} \cdot \delta(t - t_i) + \sum_{i=1}^{s} S_{t_i} \cdot \delta(t - t_i) \\ \quad + \sum_{i=s+1}^{d} D_{t_i} \cdot \delta(t - t_i), \end{cases} \tag{1}$$

A. DATA DESCRIPTION

The PV day-ahead predicted data are hourly forecast data obtained from a day-ahead prediction model that comprises a simplified PV maximum power point tracking (MPPT) estimation [27] and metadata. The metadata referring to the accumulated ground solar radiation from Météo France, is freely accessible for day-ahead predicted data and is applied in day-ahead optimization [28]. However, data of poor accuracy are sometimes missing or cannot be updated in time. The load-demand day-ahead prediction data are obtained from a load demand adjustment model that handles the metadata from Électricité De France, and the commercial building information of the staff and administrators is taken from a human-machine interface. The short-term prediction data are obtained using the short-term prediction model in Fig. 2, where a moving-average algorithm with low cost is applied because of the continuity of the load demand and weather data in this paper [29]. The measurement data include load demand data from the load power estimation and PV power data from the PV MPPT power estimation [30].

B. MOVING-AVERAGE ALGORITHM

The moving-average algorithm is introduced as a time-series prediction method [31], which can online eliminate irregular time series of changes, thus revealing a trend of time series data in Fig. 3. The algorithm is simple to apply with little calculation cost considering the statistical characteristics of time-series data.

The principle of the prediction process is shown in Fig. 3. There are two data series, namely the measurement series (Z_1, Z_2–Z_h) and prediction series (P_1, P_2–P_l). The average value of measurement series A is first calculated and then taken as the first point of the prediction series, $P1 = A$.

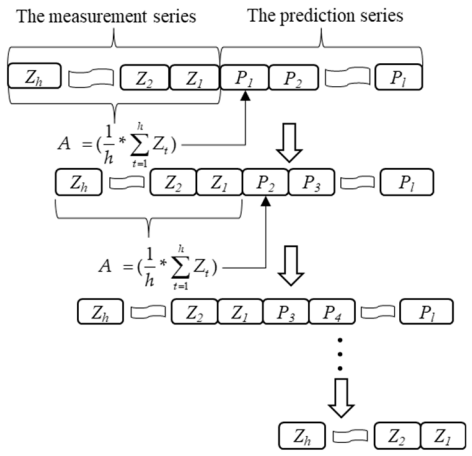

FIGURE 3. Moving-average algorithm.

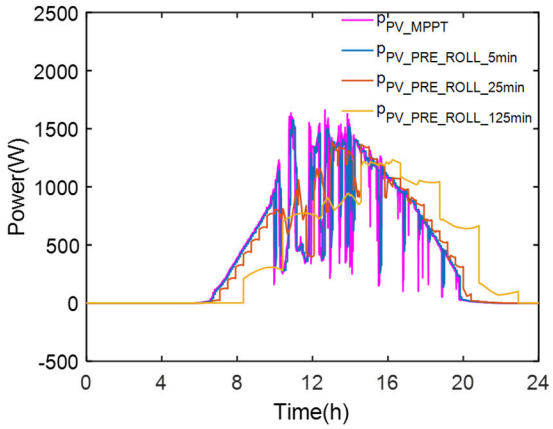

FIGURE 4. Comparison of rolling prediction results for different horizons.

The first prediction point P_1 and the measurement series (Z_{h-1}–Z_2, Z_1) are then taken as the new measurement series (Z_1, Z_2–Z_h). Finally, the calculation is repeated from the first step until the rest of the predicted series is obtained (P_2, P_3–P_l). The prediction method is suitable for short measurement series and short prediction series.

Comparison of rolling prediction results for different horizons, 5min, 25min, and 125 min, are shown in Fig. 4.

The drawback to the prediction method is that the error proportionally increases with the horizon of prediction, because the method relies heavily on historical data and drastic changes of PV power, which is difficult for a long-term prediction with this method. In this paper, the rolling prediction horizon of 5 min is chosen for the short-term prediction data.

C. DATA RESTRUCTURING

The restructured data frame at time t_0 is represented in Fig. 2, where the measurement data intercepts the segment from t_m to t_0, the short-term prediction data intercepts the segment from t_1 to t_s, and the day-ahead prediction data intercepts

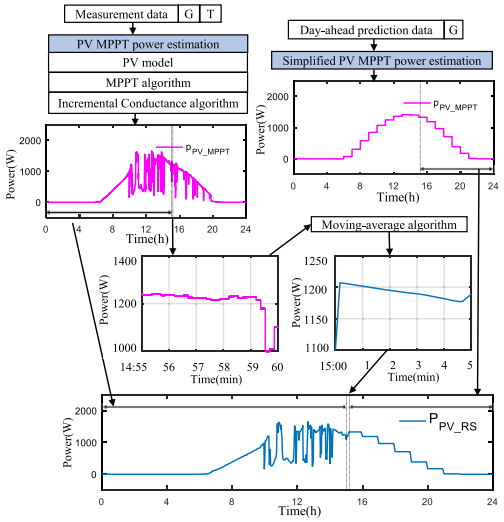

FIGURE 5. Process of reconstructing data.

the segment from t_{s+1} to t_d. An example of the process of reconstructing data for PV is given in Fig. 5, where three types of PV data—measurement data, short-term prediction data, and day-ahead prediction data—are restructured in chronological order as long-term data. The data are specifically restructured as follows. First, the PV measurement data are got by the PV MPPT power estimation model simulating with the recorded temperature and solar irradiation, because the PV MPPT power estimation model can accurately simulate the voltage and current characteristics of PV panels. Then, the PV day-ahead prediction data are provided by the simplified PV MPPT power estimation model with the hourly forecast solar irradiation data from the weather forecast agency Météo France, because the simplified PV MPPT power estimation model is fast and suitable for PV prediction. Next, the short-term prediction data are obtained by using the moving-average algorithm with the input of the PV measurement data. Finally, the three types of data are restructured to be p_{PV_RS} in chronological order. The above process takes place in a loop, and this is the online rolling method of data restructuring.

III. ONLINE MULTI-LEVEL ENERGY MANAGEMENT SYSTEM

Multiple power generation sources, storage systems, and loads make the energy management of a commercial building microgrid complicated under uncertain conditions that RESs and the load demand are separately affected by weather conditions and user behaviors. Accordingly, an online multi-level EMS that comprehensibly considers energy and power management should be established to handle the discrete events of loads and the continuous regulation of the commercial building microgrid. The structure of the online multi-level EMS comprises a physical module, controller, long-term rolling optimization level, rule-based optimization level, and load demand optimization level as shown in Fig. 6, where CB denotes commercial building, CBM represents commercial

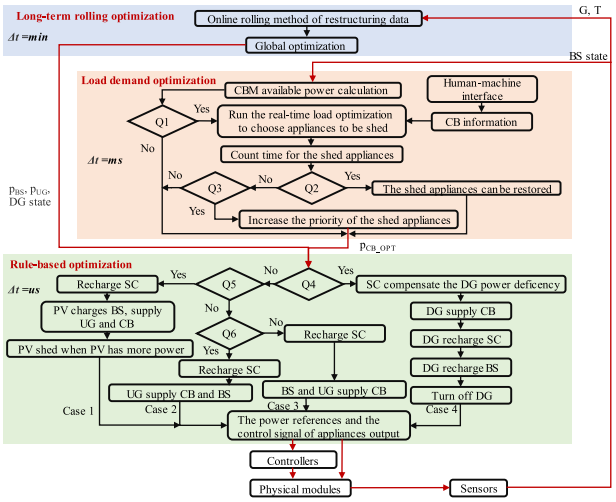

FIGURE 6. Structure of the online multi-level EMS.

TABLE 1. Question list.

Sign	Question
Q1	If load demand needs to be shed?
Q2	If the count time of the shed appliances reaches T_{min}?
Q3	If the count time of the shed appliances reaches T_{max}?
Q4	If the critical load is at risk of being shed?
Q5	If the PV power is excessive?
Q6	If UG is in power valley?

building microgrid. The long-term rolling optimization level conducts an intraday rolling global optimization by restructuring day-ahead prediction data, short-term prediction data, and measurement data. Considering the uncertainties of the users' behaviors and weather conditions, the results obtained at the long-term rolling optimization level are optimized for the second time at the rule-based optimization level, which deals with the differences (i.e., errors) between the prediction data and measurement data. The role of the real-time load demand optimization level determines the load shedding and restoration sequence, and the rule-based optimization level further ensures the rationalization of load shedding and restoration sequence, thus guaranteeing the real-time balance of the commercial building microgrid.

A question list is presented in Table 1. T_{min} is the minimal time that appliances can be shed, whereas T_{max} is the maximal time that appliances can be shed.

A. LONG-TERM ROLLING OPTIMIZATION LEVEL

The long-term rolling optimization level comprises the online rolling method of restructuring data mentioned previously and global optimization.

The global optimization modeling for the whole operation period considers all constraints of the physical components, but not constraints of the SC so as to reduce the computational complexity. The global optimization optimizes the energy cost by dispatching the power flow according to the restructured data. Considering each component cost of the commercial building microgrid, the optimization objective to minimize the total operational cost is given by

$$MinC_{TOTAL} = C_{PV\_S} + C_{CB\_S} + C_{BS} + C_{UG} + C_{DG}, \quad (2)$$

where C_{PV_S} is the energy cost adopted to punish PV shedding, C_{CB_S} is the energy cost adopted to punish load shedding, C_{BS} is the BS energy cost, C_{UG} is the UG energy cost, and C_{DG} is the DG energy cost, which comprises the fuel cost C_{DG_F} and DG operation and maintenance cost C_{DG_OM}. C_{PV_S}, C_{CB_S} are separately calculated according to the amount of PV shedding and load shedding power p_{PV_S}, p_{CB_S} and their punishment tariff T_{PV_S}, T_{CB_S} in (3) and (4); C_{BS} is denoted by its tariff T_{BS} and the absolution of its power p_{BS} in (5), and the positive/negative of p_{BS} represents the BS charging/discharging; C_{UG} is given by the negative of the UG power p_{UG} and the UG's tariff T_{UG} in (6), and the positive/negative of p_{UG} represents that the commercial building microgrid sells/buys power to/from the UG; C_{DG} consists of C_{DG_F} and C_{DG_OM} in (7), C_{DG_F} is expressed as (8) C_{DG_OM} is denoted in (9) using the DG operating time that is calculated by counting Δt when DG is turned on [32]. The rationale for setting these tariffs is to encourage the use of green energy while protecting load demand.

$$C_{PV\_S} = \sum_{t_i=t_0}^{t_F} T_{PV\_S}(t_i) \cdot \Delta t \cdot p_{PV\_S}(t_i), \quad (3)$$

$$C_{CB\_S} = \sum_{t_i=t_0}^{t_F} T_{CB\_S}(t_i) \cdot \Delta t \cdot p_{CB\_S}(t_i), \quad (4)$$

$$C_{BS} = \sum_{t_i=t_0}^{t_F} T_{BS}(t_i) \cdot \Delta t \cdot |p_{BS}(t_i)|, \quad (5)$$

$$C_{UG} = \sum_{t_i=t_0}^{t_F} T_{UG}(t_i) \cdot \Delta t \cdot (-p_{UG}(t_i)), \quad (6)$$

$$C_{DG} = C_{DG\_F} + C_{DG\_OM}, \quad (7)$$

$$C_{DG\_F} = \sum_{t_i=t_0}^{t_F} T_{DG\_F}(t_i) \cdot \Delta t \cdot p_{DG}(t_i), \quad (8)$$

$$C_{DG\_OM} = \sum_{t_i=t_0}^{t_F} T_{DG\_OM}(t_i) \cdot \Delta t \cdot (p_{DG}(t_i) > 0). \quad (9)$$

The following constraints are considered in global optimization.

The power balance constraints considering the PV sources, DG, commercial building, BS, and UG [33] are

$$p_{PV}(t_i) + p_{DG}(t_i) = p_{CB}(t_i) + p_{BS}(t_i) + p_{UG}(t_i), \quad t_i = \{t_0, t_0 + \Delta t, t_0 + 2\Delta t, \ldots, t_F\}, \quad (10)$$

where p_{PV} is the power of the PV sources; p_{DG} is the DG supply power, which is zero or positive; p_{CB} is the power required by the commercial building; p_{BS} is the BS power, which is

positive/negative for BS charging/discharging; p_{UG} is the UG power, which is positive/negative for power injection/supply; t_i denotes the times of sampling; and Δt is the time interval between two samples.

The PV power p_{PV} is constrained by its maximum generated power p_{PV_MPPT} under current solar irradiation and ambient temperature conditions, which is expressed by

$$p_{PV}(t_i) = p_{PV\_MPPT}(t_i) - p_{PV\_S}(t_i), \tag{11}$$

where p_{PV_S} is the PV shedding power.

This BS constraints are described by the following equations [33]:

$$\begin{aligned} soc_{BS}(t_i) &= SOC_{BS\_0} \\ &= \frac{1}{3600 \cdot v_{BS} \cdot C_{REF}} \sum_{t_i=t_0}^{t_F} p_{BS}(t_i)\Delta t \end{aligned} \tag{12}$$

$$SOC_{BS\_MIN} \le soc_{BS}(t_i) \le SOC_{BS\_MAX}, \tag{13}$$

$$-P_{BS\_MAX} \le p_{BS}(t_i) \le P_{BS\_MAX}. \tag{14}$$

Equation (12) expresses the soc_{BS} estimation method. soc_{BS} refers to the real-time state of charge (SOC) of the BS, $SOC_{BS\_MIN}/SOC_{BS\_MAX}$ is the lowest/highest point of BS discharge/charging in (13). P_{BS_MAX} is the maximum power of the BS charging or discharge, which reflects the maximum current of the BS in (14).

The UG is assumed to be a single utility grid connection, whose constraints are expressed as

$$-P_{UG\_MAX} \le p_{UG}(t_i) \le P_{UG\_MAX}, \tag{15}$$

$$|p_{UG}(t_i) - p_{UG}(t_{i-1})| \le P_{UG\_FLUC}, \tag{16}$$

where p_{UG} is limited by P_{UG_MAX} in (15) and the UG power fluctuation is limited to P_{UG_FLUC} in (16) to protect the UG power quality.

The DG constraint is denoted by (17). The on/off status of the DG can be determined when t_i is an integer multiple of dt_{DG}. p_{DG} is zero when the DG is off, and p_{DG} is limited between the minimal DG output power $P_{DG\_ON\_MIN}$ and maximal DG output power $P_{DG\_ON\_MAX}$ when the DG is on:

$$p_{DG}(t_i) = p_{DG}(t_{i-1}) \begin{cases} if\ rem(t_i/dt_{DG}) \neq 0, \\ p_{DG}(t_i) \in \{0\} \cup \\ \left[p_{DG\_ON\_MIN} \quad p_{DG\_ON\_MAX}\right]. \end{cases} \tag{17}$$

The load demand of the building p_{CB_D}, is assumed to comprise the critical load p_{CB_CRT} and non-critical load $p_{CB\_N\_CRT}$ in (18). p_{CB} and its power shedding p_{CB_S} are limited by p_{CB_D}:

$$p_{CB\_D} = p_{CB\_CRT} + p_{CB\_N\_CRT}, \tag{18}$$

$$p_{CB}(t_i) = p_{CB\_D}(t_i) - p_{CB\_S}(t_i). \tag{19}$$

The DG is designed to support the peak load independently, with aim of characterizing the off-grid operation of the commercial building microgrid, thus the UG is restricted to 0 when the high-cost DG is turned on:

$$if\ p_{DG}(t_i) > 0\ then\ p_{UG}(t_i) = 0. \tag{20}$$

BS is available to offset some but not all of the PV production and load demand. The PV supply and loads cannot be shed when the BS is available:

$$if\ soc_{BS}(t_i) > SOC_{BS\_MIN}\ then\ p_{CB\_S}(t_i) = 0, \tag{21}$$

$$\begin{aligned} &if\ soc_{BS}(t_i) < SOC_{BS\_MAX} \text{ and } p_{DG}(t_i) = 0 \\ &then p_{PV\_S}(t_i) = 0. \end{aligned} \tag{22}$$

There are additional constraints under two conditions. Constraints (23) are applied at the UG power shoulder and peak and constraints (24) are applied in the UG power valley:

$$\begin{cases} a \begin{cases} if\ p_{PV\_MPPT}(t_i) \ge p_{CB\_D}(t_i),\ then \\ \begin{cases} p_{UG}(t_i) \ge 0 \\ p_{BS}(t_i) \ge 0 \end{cases} \end{cases} \\ b \begin{cases} if\ p_{PV\_MPPT}(t_i) \le p_{CB\_D}(t_i)\ and \\ p_{DG}(t_i) = 0,\ then \begin{cases} p_{UG}(t_i) \le 0 \\ p_{BS}(t_i) \le 0 \end{cases} \end{cases} \\ c \left\{p_{CB\_S}(t_i) \le (1 - k_{CB\_CRIT}) \cdot p_{CB\_D}(t_i)\right. \end{cases} \tag{23}$$

$$p_{CB\_S}(t_i) \le (1 - k_{CB\_CRIT}) \cdot p_{CB\_D}(t_i). \tag{24}$$

Equations (23)a and (23)b together constrain that the BS and UG cannot directly exchange power at the UG power shoulder and peak, and (23)c constrains the load shedding power by a critical load coefficient, k_{CB_CRIT}. Equation (24) only constrains the load shedding power, thus the BS and UG can exchange power in the UG power valley.

B. LOAD DEMAND OPTIMIZATION LEVEL

The objective of the load demand optimization is to maximize the priority coefficient sum of the operating appliances $f(S_{Ap})$ to protect important critical loads in (25), where i is the appliance number. Cop_i is the coefficient of priority of the i^{th} appliance. S_{Ap_i} is the decision variable of the load demand optimization. S_{Ap_i} is 0 when the i^{th} appliance is off; S_{Ap_i} is 1 when the i^{th} appliance is on. The constraint is in (26), where $p_{CB\_}$ is limited by the minimal value of p_{CB_D} and the available power of the commercial building microgrid, p_{Avial}, supplied by the PV sources, UG, BS, DG, and SC.

$$\begin{aligned} \text{Max } f(S_{Ap}) &= \sum_{i=1}^{n} Cop_i * S_{Ap\_i} \\ &\begin{cases} S_{Ap\_i} = \begin{cases} 0 & \text{if } i^{th} \text{ appliance is off} \\ 1 & \text{if } i^{th} \text{ appliance is on} \end{cases} \\ i = \{1, 2, 3, \ldots, n\}, \end{cases} \end{aligned} \tag{25}$$

$$p_{CB} \le \min(p_{CB\_D}, p_{Avial}). \tag{26}$$

Fig. 7 is the flow diagram of the load demand optimization. The process of optimizing the load demand is as follows. The microgrid operator of a commercial building judges if the load demand needs to be shed. If p_{Avial} is less than p_{CB_D}, then the optimization objective (25) is run to choose the proper appliances to be shed. Meanwhile, the time of shedding appliances is counted. The appliances remain shed if the counted

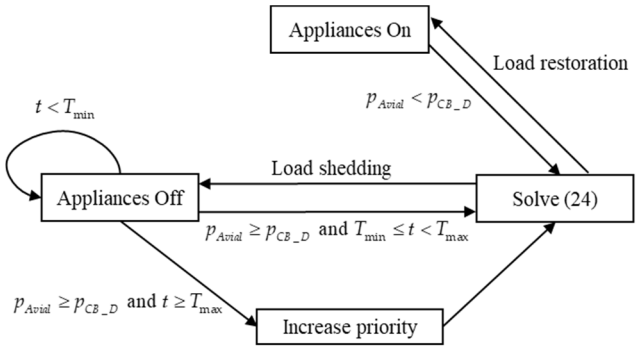

FIGURE 7. Flow diagram of the load demand optimization.

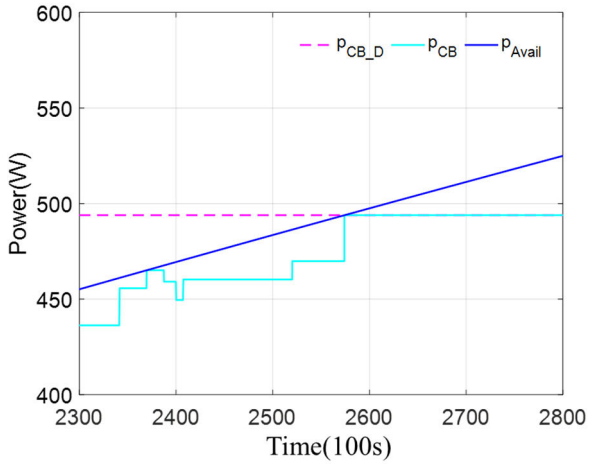

FIGURE 8. Simulation results of real-time load optimization.

time for the shed appliances is less than T_{min}. There are two paths for load restoration. One is when p_{Avial} is greater than p_{CB_D}, the appliances can be restored if the count time for the shed appliances is greater than T_{min}. The other is the priority of the shed appliances is increased to forcibly restore the shed appliances if their count time reaches T_{max}. The load demand optimization operates continually as the above processes until the simulation is complete.

Fig. 8 presents simulation results of the load demand optimization. When the curve of p_{Avial} is below the curve of p_{CB_D}, p_{CB} is below the curve of p_{Avial}, which shows that the real-time load optimization is running to shed some proper appliances. When the curve of p_{Avial} is above the curve of p_{CB_D}, all the load power demand can be met, and the curves of p_{CB_D} and p_{CB} thus coincide.

C. RULE-BASED OPTIMIZATION LEVEL

The rule-based optimization level redistributes the energy flow of the microgrid and controls the appliances by reading the output results of the long-term rolling optimization level and load demand optimization level.

Rules are designed as follows to ensure optimal real-time energy allocation.

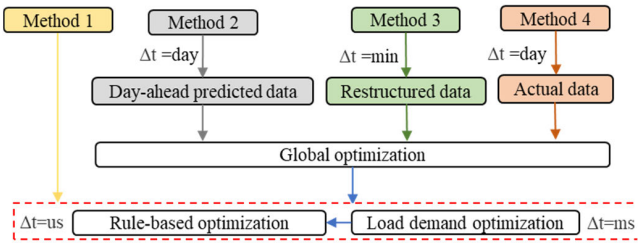

FIGURE 9. Demonstration flow diagram of four designed methods.

Cases 1, 2, and 3 differ from case 4 according to the question of whether a critical load will be shed (Q4), as shown in Fig. 6. Case 1 is that the PV sources generate excess power. The excess power charges the BS or is sold to the UG according to the optimization results of the long-term rolling optimization level. There may even be a direct PV shedding operation. Cases 2 and 3 are that the PV supply is insufficient to supply loads. Case 2 differs from case 3 in terms of distributing the power flow according to the question of whether the UG is in a power valley (Q6). In case 2, the UG is in a power valley with a low-price cost and can supply loads and the BS. In case 3, the BS and UG can supply loads according to the long-term rolling optimization level results. Case 4 is that a critical load is at risk of being shed. Ultimately, the power references of the PV sources, BS, UG, SC, DG, and the control signal of the loads are output to control the microgrid state.

IV. SIMULATION

The EMS is programmed in MATLAB/Simulink, and the optimization is solved using CPLEX [34]. Four methods are designed and compared to choose the optimal method for EMS in terms of the utilization rate of PV sources and the cost of the commercial building microgrid. Fig. 9 is a demonstration flow diagram of the four methods.

Method 1 combines the rule-based optimization and load demand optimization. Methods 2, 3, and 4 are designed in the same way by combining rule-based optimization, load demand optimization, and global optimization. In particular, the input of Method 2 is the day-ahead prediction data that are updated daily; the input of Method 3 is the restructured data obtained using the online rolling method of data restructuring, where the restructured data are updated in minutes; and the input of Method 4 is the actual data assumed to be accessed in the simulation without the predictive accuracy problem.

A. SCENARIO DESIGN AND PARAMETERS

The simulation scenario is designed for an operational period of 24 h, which is separated into five time periods: 0:00–6:00, 6:00–8:00, 8:00–17:00, 17:00–22:00, and 22:00–24:00. A commercial building environment on a summer day in France is simulated. The roof-top PV sources comprise 14 PV panels (SF 130/2-125, Solar-Fabrik, Germany) arranged in series, whose maximum power output is 1750 W

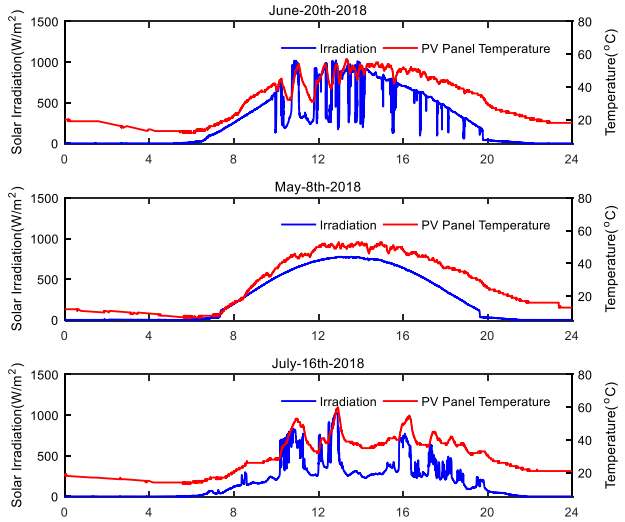

FIGURE 10. Three weather data recording.

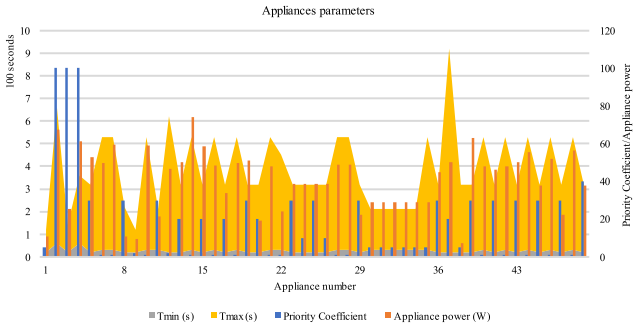

FIGURE 11. Appliances parameters.

under standard test conditions. Three weather data recording are shown in Fig. 10. June 20th 2018, May 8th 2018, and July 16th 2018 in France were cloudy, sunny, rainy days, respectively [33]. The UG is a single-phase voltage power source. The BS comprises five lead-acid batteries arranged in series, whose individual specifications are 12 V/6.6 Ah. The DG used in this simulation is an SDMO Technic 6500 E AVR. The SC has a capacity of 94 F and rated voltage of 75 V.

The studied microgrid is designed for real application based on a commercial building with 100 kW load demand. The load power curve coming from an office building in France, is scaled to an experimentally verifiable scale for 49 appliances, including emergency lighting, a stair lift, multiple personal computers, multiple printers, and other electrical equipment. Fig. 11 presents the appliance parameters defined by staff and administrators, including the shed time constraints, the rated power of the appliances, and the shed priority coefficient. Additionally, the time constraints are defined to reflect the dynamic characteristics of user behaviors. The maximal priority coefficient is 100, and the minimal priority coefficient is 1.

Table 2 presents the five-time periods [33]. During the periods 0:00–6:00 and 22:00–24:00, the commercial building

TABLE 2. Scenario parameters.

Period	Description	Power strategy	Constraints
22:00-6:00 (Power valley)	Low load demand	Cases 1,3,4	(24)
6:00-8:00	Varies according to seasons	Cases 1,2,4	(23)
8:00-17:00	Working time in building		
17:00-22:00	High load demand from the UG		

has a low load demand, and it is assumed that the commercial building maintains all critical loads, respecting the additional constraints in (24) and power strategies in cases 1, 3, and 4, to encourage the UG to discharge and smooth its power valley. During the period 6:00–8:00, the PV energy production and load demand vary according to the season. It is assumed that the additional constraints in (23) and power strategies in cases 1, 2, and 4 are applied to prevent the power exchange between the UG and BS and thus prevent the microgrid administrator from using the BS to profit from the UG to aggravate the instability of the UG by buying electricity at a low price and selling at a high price during the day. During the period 8:00–17:00, the load demand varies according to the user behaviors, and the EMS is assumed to use the additional constraints in (23) and the strategies in cases 1, 2, and 4 to coordinate power flow for the microgrid. During the period 17:00–22:00, the load demand is low for commercial buildings but high for residential buildings, and the UG is thus highly stressed locally. The additional constraints in (23) and the strategies in cases 1, 2, and 4 are thus assumed to apply.

The simulation parameters are given in Table 3 [33]. The initial SOC of the BS, SOC_{BS_0}, is set at 50%. p_{BS} is limited to 1000 W, and soc_{BS} is limited to the range of 20%–80%, which alleviates BS aging. Considering the efficiency of power conversion between the microgrid and UG, the reference voltage of the common DC bus, v^*_{DC}, is set at 400 V. P_{UG_MAX} is limited to 600 W in the power valley and 200 W in other power periods. The proportion of critical loads, k_{L_CRIT}, is assumed to be 100% approximately at night and 80% at other times, indicating that the shadow rate of the load demand is 0% at night and not greater than 20% at other times. p_{DG} is limited to 1500 W to satisfy the maximal load demand power. P_{SC_MAX} is set at 1500 W to compensate for the DG power deficiency during the start-on stage, and the initial SOC of the SC, SOC_{SC_0}, is 75%.

The tariff of each physical component is predefined according to a selected pricing mechanism, where the high load shedding punishment tariff is set at 1.8 €/kWh, the PV power shedding punishment tariff is set at 1.5 €/kWh, the UG power tariff is set using the TOU method [35], the BS power tariff is set considerably low at 0.05 €/kWh, the DG power tariff is contrastively set high at 1.2 €/kWh owing to the high

TABLE 3. Simulation parameters.

Parameter	Value	Parameter	Value
P_{BS_MAX}	1000W	k_{L_CRIT}	80% or 100%
SOC_{BS_MAX}	80%	P_{DG_MAX}	1500W
SOC_{BS_MIN}	20%	P_{UG_MAX}	200W or 600W
SOC_{BS_0}	50%	SOC_{SC_0}	75%
v^*_{DC}	400V	P_{SC_MAX}	1500W

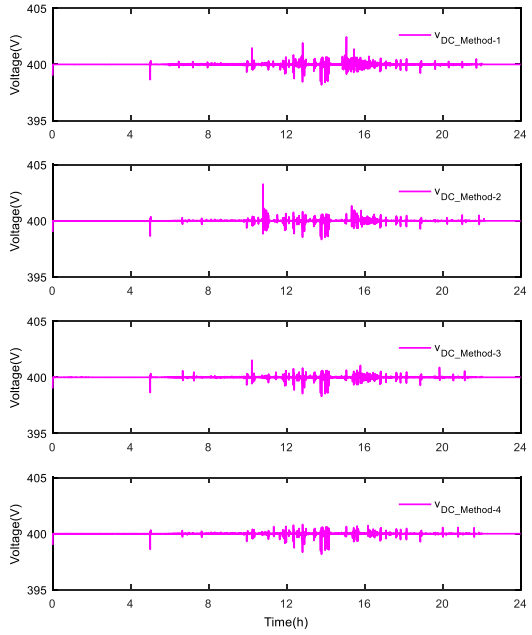

FIGURE 12. DC bus curves obtained using the four designed methods.

cost of fuel, and the DG operation and maintenance tariff is set at 0.63 €/kWh [32].

B. SIMULATION RESULTS AND ANALYSIS

Methods 1, 2, 3, and 4 are applied in the simulation to comprehensively compare their operational feasibility, load power rate, PV power usage rate, and operational cost, where data conditions of Method 4 are ideal. The detailed operating status of the commercial building microgrid on June 20, 2018 is shown from Fig. 12 to Fig. 17.

The DC bus voltage of each method is shown in Fig. 12. This figure shows that the microgrid of a commercial building can operate well under each method while keeping the DC bus voltage stable.

The PV power curve is shown for each method in Fig. 13, where the PV installed capacity is represented by the red dotted line. At night, the energy generated by PV sources is nearly zero. During the day, the generation of PV power gradually increases until it reaches a maximum at noon and then gradually decreases. The violent energy fluctuation is

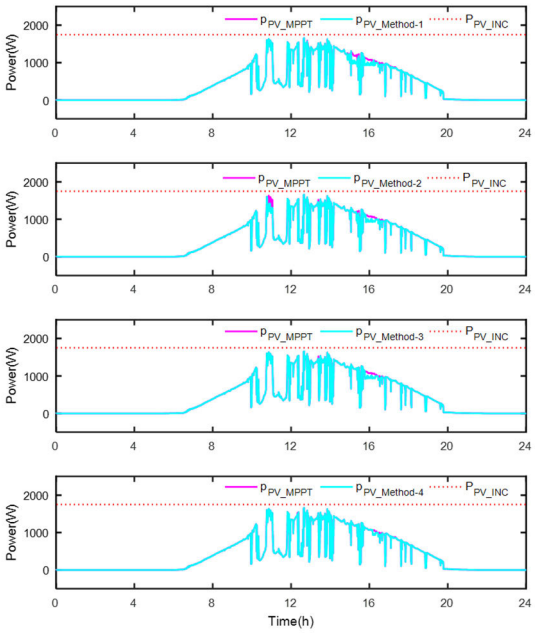

FIGURE 13. PV curves obtained using the four designed methods.

mainly due to the variation in shading by moving clouds. Under the four methods, the PV sources operate well in the PV MPPT mode and PV shedding mode.

Fig.14 presents the load demand power and operational load power greater or equal to the critical load power drawn as the red dotted line. At night, all loads that need to be run are set as critical loads to ensure the minimum operating requirements of the commercial building. During the day, with an increase in the staffing level, the load of the commercial building gradually increases until reaching a maximum at noon and then decreases with the gradual departure of staff.

Fig. 15 reveals the power charging, power discharging, and SOC evaluations of the BS under all limitations. At night, the BS tends to charge owing to the low electricity price of the UG. During the day, the complex change in the BS state is mainly due to the intermittence of PV power generation and load demand.

Fig.16 presents the UG power, which operates within power limitations. At night, the UG, limited to 600 W, tends to sell energy at a low price to smooth its power valley. During the day, the UG power limitation is set at 200 W to ensure the stable operation of the commercial building microgrid.

Fig. 17 gives the operating results of the DG and SC. At night, the DG hardly runs owing to the low load demand and low UG price. During the day, the DG participates in the energy supply as a high-price source and serves as a final means to maintain the energy balance for the microgrid. The start-up of the DG is always accompanied by an energy supplement of the SC. The SC needs to be charged when its SOC is low to prevent its discharging.

The PV power usage rate and load power rate of three weather conditions are shown for each method in Fig. 18.

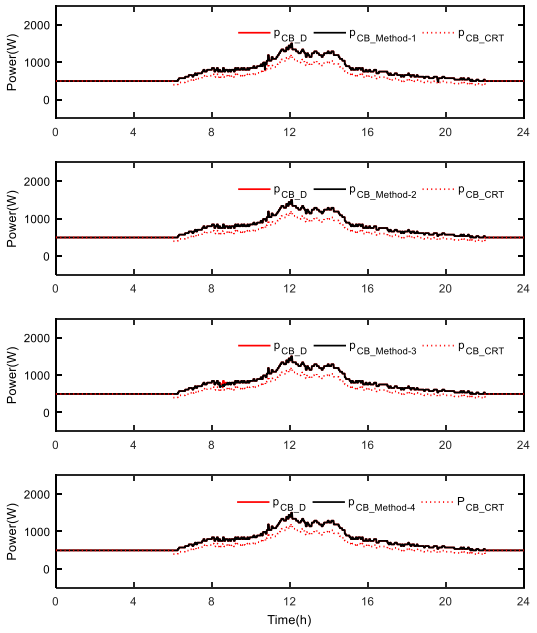

FIGURE 14. **Power curves of a commercial building obtained using the four designed methods.**

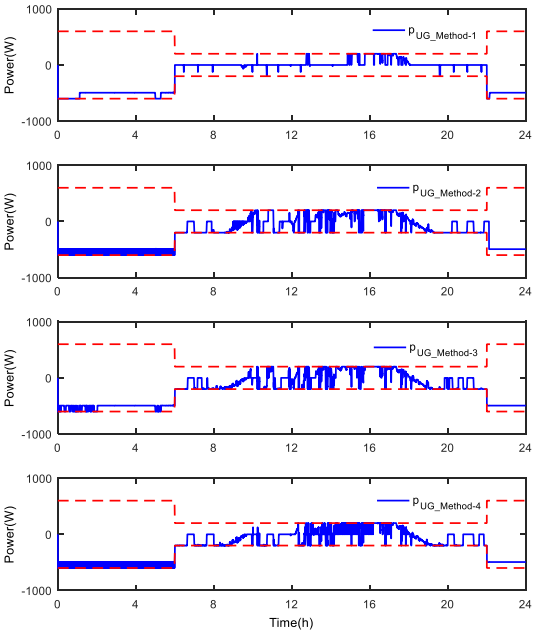

FIGURE 16. **UG curves obtained using the four designed methods.**

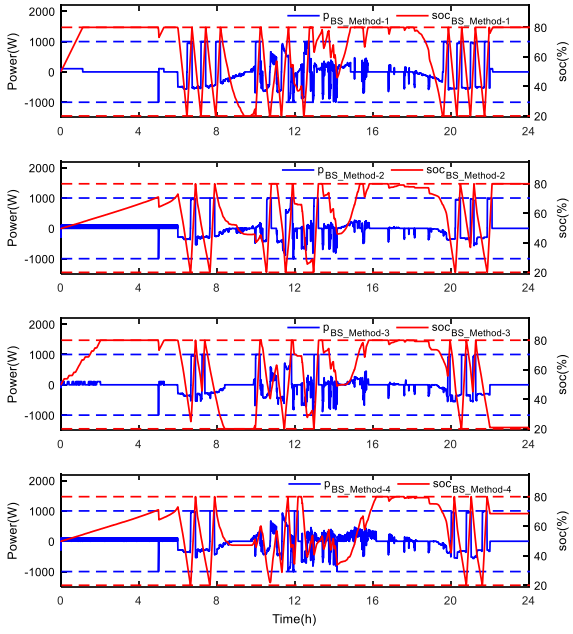

FIGURE 15. **BS curves obtained using the four designed methods.**

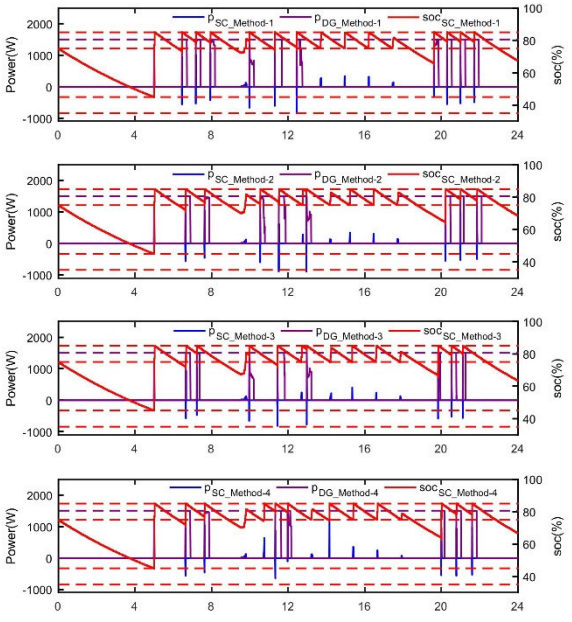

FIGURE 17. **DG and SC curves obtained using the four designed methods.**

The PV power usage rate and load power rate under the three weather conditions is gradually increased from Method 1 to Method 4, and the special case was on June 20, 2018, where the load power rate of Method 3 was lower than that of Methods 1, 2 and 4, which was due to the time gap encountered for the DG restart, and the non-critical load was shed.

On June 20, 2018, PV power has the lowest usage rate, 98.13%, for Method 1 and the highest usage rate, 99.68%, for Method 4. Method 2 has a higher PV power usage rate, 98.53%, than Method 1. Moreover, Method 3 has a higher usage rate of PV power, 99.22%, than Methods 1 and 2; the rate is nearly as high as that for Method 4. The load power rate of methods 1, 2, 3, and 4 are 99.97%, 100%, 99.87%, and 100%, respectively.

On May 8, 2018, PV power has the lowest usage rate, 99.89%, for Method 1 and the highest usage rate, 99.99%,

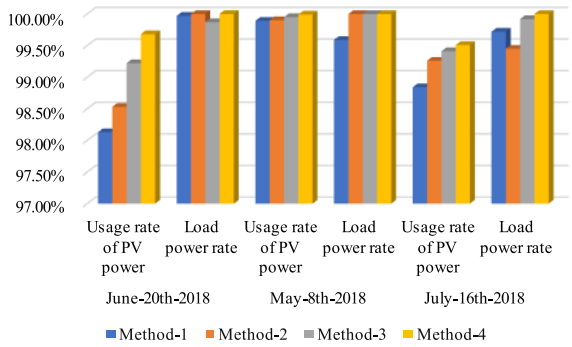

FIGURE 18. **PV power usage rate and load power rate comparison.**

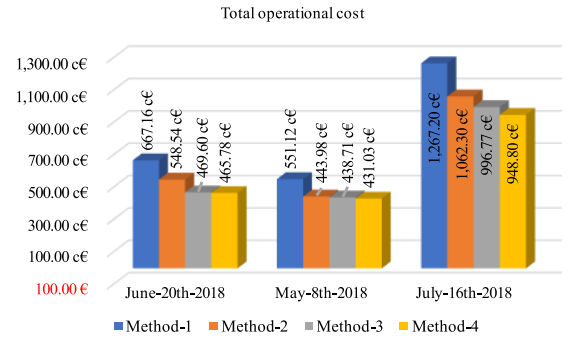

FIGURE 19. **Total cost comparison.**

for Method 4. Method 2 has a higher PV power usage rate, 99.90%, than Method 1. Moreover, Method 3 has a higher usage rate of PV power, 99.95%, than Methods 1 and 2; the rate is nearly as high as that for Method 4. The load power rate of methods 1, 2, 3, and 4 are 99.59%, 100%, 100%, and 100%, respectively.

On July 16, 2018, PV power has the lowest usage rate, 98.84%, for Method 1 and the highest usage rate, 99.51%, for Method 4. Method 2 has a higher PV power usage rate, 99.26%, than Method 1. Moreover, Method 3 has a higher usage rate of PV power, 99.41%, than Methods 1 and 2; the rate is nearly as high as that for Method 4. The load power rate of methods 1, 2, 3, and 4 are 99.72%, 99.85%, 99.92%, and 100%, respectively.

These results indicate that Method 3 performs better than Methods 1 and 2 in terms of PV power usage, while the load power rate of Method 3 is similar to the rates for the other three methods.

Fig. 19 presents the total costs of using the four methods of three weather conditions. The total costs under the three weather conditions are gradually reduced from Method 1 to Method 4.

On June 20, 2018, the total cost of Method 2 is 17.78% less than that of Method 1. The total cost of Method 3 is 29.61% less than that of Method 1 and almost the same as that of Method 4.

On May 8, 2018, the total cost of Method 2 is 19.44% less than that of Method 1. The total cost of Method 3 is 20.40% less than that of Method 1 and almost the same as that of Method 4.

On July 16, 2018, the total cost of Method 2 is 16.17% less than that of Method 1. The total cost of Method 3 is 21.34% less than that of Method 1 and almost the same as that of Method 4.

The above results demonstrate that the four methods ensure the normal operation of the commercial building microgrid. Additionally, Method 3 performs well in reducing the operational cost and improving the utilization rate of PV sources.

V. CONCLUSION

This paper investigated an EMS for a commercial building microgrid to improve the utilization rate of PV sources and reduce the cost of the commercial building microgrid on the premise of ensuring the stability of the power supply system. The EMS mainly comprises a long-term rolling optimization level, rule-based optimization level, and load demand optimization level. The rule-based optimization level coordinates the energy flow for the commercial building microgrid, the load demand optimization level maximizes the sum of the coefficients of priorities under the available power limit, and the long-term rolling optimization level schedules a long-term proper power flow for the commercial building microgrid. Moreover, an online rolling method of data restructuring was developed to improve the uncertainty in PV power generation and load demand in the long-term rolling optimization level. The method can operate over multiple cycles on the whole-day timescale.

On the cloudy day, Method 3 effectively improves the utilization rate of PV sources by 1.09%, while reducing the total cost by more than 29.61% for the commercial building microgrid with only small effects on the loads compared with Methods 1 and 2; On the sunny day, Method 3 effectively improves the utilization rate of PV sources by 0.06%, while reducing the total cost by more than 20.40% for the commercial building microgrid; On the rainy day, Method 3 effectively improves the utilization rate of PV sources by 0.57%, while reducing the total cost by more than 21.30% for the commercial building microgrid. The above simulation results demonstrate that the EMS operates well for the commercial building microgrid, which provides a theoretical basis for energy management and optimal dispatch of commercial building microgrids in the future, such as office buildings, bank buildings, shopping mall buildings, etc.

Adjustable loads are not considered in this paper because adjustable loads such as those of the EVs need to be studied in dedicated works owing to the complexity of their behavioral characteristics. Future work will focus on the research of the management strategy for the commercial building microgrid integrating EVs, making full use of the source–load characteristics of EVs to charge EVs in the period of PV power generation or the power valley of the UG. Additionally, future work will investigate discharge to the commercial building

microgrid in the period of the power peak of the UG, which can alleviate pressure on the UG, benefit EV users, and, importantly, provide a path for the future design of net-zero buildings.

REFERENCES

[1] *Energy Technology Perspectives 2020*, IEA, Paris, France, 2020. [Online]. Available: https://www.iea.org/reports/energy-technology-perspectives-2020

[2] *Tracking Buildings 2020*, IEA, Paris, France, 2020. [Online]. Available: https://www.iea.org/reports/tracking-buildings-2020

[3] F. Rahmani, M. A. Robinson, and M. R. Barzegaran, "Cool roof coating impact on roof-mounted photovoltaic solar modules at Texas green power microgrid," *Int. J. Electr. Power Energy Syst.*, vol. 130, Sep. 2021, Art. no. 106932.

[4] W. Su, J. Wang, and J. Roh, "Stochastic energy scheduling in microgrids with intermittent renewable energy resources," *IEEE Trans. Smart Grid*, vol. 5, no. 4, pp. 1876–1883, Jul. 2014.

[5] Z. Wang, C. Shen, Y. Xu, F. Liu, X. Wu, and C.-C. Liu, "Risk-limiting load restoration for resilience enhancement with intermittent energy resources," *IEEE Trans. Smart Grid*, vol. 10, no. 3, pp. 2507–2522, May 2019.

[6] Z. Liang, H. Chen, X. Wang, S. Chen, and C. Zhang, "Risk-based uncertainty set optimization method for energy management of hybrid AC/DC microgrids with uncertain renewable generation," *IEEE Trans. Smart Grid*, vol. 11, no. 2, pp. 1526–1542, Mar. 2020.

[7] F. Fallahi, M. Yildirim, J. Lin, and C. Wang, "Predictive multi-microgrid generation maintenance: Formulation and impact on operations & resilience," *IEEE Trans. Power Syst.*, vol. 36, no. 6, pp. 4979–4991, Nov. 2021.

[8] P. Xie, Y. Jia, H. Chen, J. Wu, and Z. Cai, "Mixed-stage energy management for decentralized microgrid cluster based on enhanced tube model predictive control," *IEEE Trans. Smart Grid*, vol. 12, no. 5, pp. 3780–3792, Sep. 2021.

[9] Z. Chu, N. Zhang, and F. Teng, "Frequency-constrained resilient scheduling of microgrid: A distributionally robust approach," *IEEE Trans. Smart Grid*, vol. 12, no. 6, pp. 4914–4925, Nov. 2021.

[10] F. Luo, G. Ranzi, S. Wang, and Z. Y. Dong, "Hierarchical energy management system for home microgrids," *IEEE Trans. Smart Grid*, vol. 10, no. 5, pp. 5536–5546, Sep. 2019.

[11] M. MansourLakouraj, H. Niaz, J. J. Liu, P. Siano, and A. Anvari-Moghaddam, "Optimal risk-constrained stochastic scheduling of microgrids with hydrogen vehicles in real-time and day-ahead markets," *J. Cleaner Prod.*, vol. 318, Oct. 2021, Art. no. 128452.

[12] M. Nikzad and A. Samimi, "Integration of designing price-based demand response models into a stochastic bi-level scheduling of multiple energy carrier microgrids considering energy storage systems," *Appl. Energy*, vol. 282, Jan. 2021, Art. no. 116163.

[13] C. Wu, S. Gao, Y. Liu, T. E. Song, and H. Han, "A model predictive control approach in microgrid considering multi-uncertainty of electric vehicles," *Renew. Energy*, vol. 163, pp. 1385–1396, Jan. 2021.

[14] F. Jiao, C. Ji, Y. Zou, and X. Zhang, "Tri-stage optimal dispatch for a microgrid in the presence of uncertainties introduced by EVs and PV," *Appl. Energy*, vol. 304, Dec. 2021, Art. no. 117881.

[15] R. Chang, L. Bai, and C.-H. Hsu, "Solar power generation prediction based on deep learning," *Sustain. Energy Technol. Assessments*, vol. 47, Oct. 2021, Art. no. 101354.

[16] E. Jumin, F. B. Basaruddin, Y. B. M. Yusoff, S. D. Latif, and A. N. Ahmed, "Solar radiation prediction using boosted decision tree regression model: A case study in Malaysia," *Environ. Sci. Pollut. Res.*, vol. 28, no. 21, pp. 26571–26583, Jun. 2021.

[17] Y. Li, R. Wang, and Z. Yang, "Optimal scheduling of isolated microgrids using automated reinforcement learning-based multi-period forecasting," *IEEE Trans. Sustain. Energy*, vol. 13, no. 1, pp. 159–169, Jan. 2022.

[18] Q. Meng, Y. Xi, X. Ren, H. Li, L. Jiang, and L. Yang, "Thermal energy storage air-conditioning demand response control using Elman neural network prediction model," *Sustain. Cities Soc.*, vol. 76, Jan. 2022, Art. no. 103480.

[19] M. Alramlawi and P. Li, "Design optimization of a residential PV-battery microgrid with a detailed battery lifetime estimation model," *IEEE Trans. Ind. Appl.*, vol. 56, no. 2, pp. 2020–2030, Mar. 2020.

[20] M. Zachar and P. Daoutidis, "Scheduling and supervisory control for cost effective load shaping of microgrids with flexible demands," *J. Process Control*, vol. 74, pp. 202–214, Feb. 2019.

[21] S. Ferahtia, A. Djeroui, H. Rezk, A. Houari, S. Zeghlache, and M. Machmoum, "Optimal control and implementation of energy management strategy for a DC microgrid," *Energy*, vol. 238, Jan. 2022, Art. no. 121777.

[22] E. Rezaei and H. Dagdougui, "Optimal real-time energy management in apartment building integrating microgrid with multizone HVAC control," *IEEE Trans. Ind. Informat.*, vol. 16, no. 11, pp. 6848–6856, Nov. 2020.

[23] K. Antoniadou-Plytaria, D. Steen, L. A. Tuan, O. Carlson, and M. A. F. Ghazvini, "Market-based energy management model of a building microgrid considering battery degradation," *IEEE Trans. Smart Grid*, vol. 12, no. 2, pp. 1794–1804, Mar. 2021.

[24] M. K. Daryabari, R. Keypour, and H. Golmohamadi, "Robust self-scheduling of parking lot microgrids leveraging responsive electric vehicles," *Appl. Energy*, vol. 290, May 2021, Art. no. 116802.

[25] Q. Wen, G. Liu, W. Wu, and S. Liao, "Genetic algorithm-based operation strategy optimization and multi-criteria evaluation of distributed energy system for commercial buildings," *Energy Convers. Manage.*, vol. 226, Dec. 2020, Art. no. 113529.

[26] K. Thirugnanam, M. S. El Moursi, V. Khadkikar, H. H. Zeineldin, and M. A. Hosani, "Energy management strategy of a reconfigurable grid-tied hybrid AC/DC microgrid for commercial building applications," *IEEE Trans. Smart Grid*, vol. 13, no. 3, pp. 1720–1738, May 2022.

[27] S. M. Hakimi, A. Hasankhani, M. Shafie-khah, and J. P. S. Catalão, "Stochastic planning of a multi-microgrid considering integration of renewable energy resources and real-time electricity market," *Appl. Energy*, vol. 298, Sep. 2021, Art. no. 117215.

[28] W. Bai, M. Sechilariu, and F. Locment, "On-grid/off-grid DC microgrid optimization and demand response management," in *Proc. 22nd Eur. Conf. Power Electron. Appl. (EPE ECCE Europe)*, Lyon, France, Sep. 2020, pp. 1–10.

[29] A. Tuohy et al., "Solar forecasting: Methods, challenges, and performance," *IEEE Power Energy Mag.*, vol. 13, no. 6, pp. 50–59, Nov. 2015.

[30] E. Manuel Godinho Rodrigues, R. Godina, M. Marzband, and E. Pouresmaeil, "Simulation and comparison of mathematical models of PV cells with growing levels of complexity," *Energies*, vol. 11, no. 11, p. 2902, Oct. 2018.

[31] G. Janacek, "Time series analysis forecasting and control," *J. Time Ser. Anal.*, vol. 31, no. 4, p. 303, Dec. 2009.

[32] C. Yin, H. Wu, M. Sechilariu, and F. Locment, "Power management strategy for an autonomous DC microgrid," *Appl. Sci.*, vol. 8, no. 11, p. 2202, Nov. 2018.

[33] W. Bai, M. Sechilariu, and F. Locment, "DC microgrid system modeling and simulation based on a specific algorithm for grid-connected and islanded modes with real-time demand-side management optimization," *Appl. Sci.*, vol. 10, no. 7, p. 2544, Apr. 2020.

[34] (2021). *CPLEX*. [Online]. Available: https://www.ibm.com/

[35] Z. Pei, M. Wan, Z.-Z. Jiang, Z. Wang, and X. Dai, "An approximation algorithm for unrelated parallel machine scheduling under TOU electricity tariffs," *IEEE Trans. Autom. Sci. Eng.*, vol. 18, no. 2, pp. 743–756, Apr. 2021.

WENSHUAI BAI received the Ph.D. degree in electrical engineering from the Université de Technologie de Compiègne, Compiègne, France, in 2021. He is currently a Lecturer with the School of Artificial Intelligence, Beijing Technology and Business University, Beijing, China. His research interests include microgrid planning and operation, power system uncertainty analysis and modeling, renewable energy modeling, and the interaction between electric vehicle and smart grid.

DIAN WANG received the Ph.D. degree in electrical engineering from the Université de Technologie de Compiègne, Compiègne, France, in 2021. She is currently an Analyst with the Energy Internet Research Department, State Grid Energy Research Institute Company Ltd., Beijing, China. Her research interests include microgrid planning and operation, multi-energy microgrid, energy policy, renewable energy modeling, and microgrid integrated with electric vehicle.

XIAORONG SUN received the B.S. degree from the Taiyuan University of Technology, Shanxi, China, in 1999, and the M.S. degree from the China University of Mining and Technology in 2003. Since 2012, she has been an Associate Professor with the Beijing Technology and Business University. Since 2021, she has been a Professor with the Beijing Technology and Business University. Her current research interests include near-infrared spectroscopic detection, determination of flour quality, and identification of flours.

JIABIN YU received the B.S. degree from the Beijing Technology and Business University, Beijing, China, in 2007, the M.S. degree in automation from the Beijing Institute of Technology in 2009, and the Ph.D. degree in control theory and control engineering from the Institute of Automation, Chinese Academy of Sciences, in 2012. Since 2017, he has been an Associate Professor with the Beijing Technology and Business University. His current research interests include water environment evaluation and prediction, motor control, and complex system design.

JIPING XU received the B.S. and M.S. degrees from the Beijing Technology and Business University, Beijing, China, in 2002 and 2005, respectively, and the Ph.D. degree from the Beijing Institute of Technology in 2008. Since 2010, he has been an Associate Professor with the Beijing Technology and Business University. His current research interests include blockchain and industrial internet identity resolution.

YUQING PAN received the B.S. degree from the Beijing Technology and Business University in 1994 and the M.S. degree in economics from the Capital University of Economics and Business in 2003. Since 2000, he has been a Lecturer with the Beijing Technology and Business University. His current research interests include neural networks and deep learning.